CHEMISTRY OF MATERIALS

Article

pubs.acs.org/cm

Nanostructuring of β-MnO_2: The Important Role of Surface to Bulk Ion Migration

David A. Tompsett,*[,†] Steve C. Parker,[†] Peter G. Bruce,[‡] and M. Saiful Islam*[,†]

[†]Department of Chemistry, University of Bath, Bath BA2 7AY, U.K., and

[‡]School of Chemistry, University of St. Andrews, Fife, KY16 9ST, U.K.

ABSTRACT: Manganese oxide materials are attracting considerable interest for clean energy storage applications such as rechargeable Li ion and Li−air batteries and electrochemical capacitors. The electrochemical behavior of nanostructured mesoporous β-MnO_2 is in sharp constrast to the bulk crystalline system, which can intercalate little or no lithium; this is not fully understood on the atomic scale. Here, the electrochemical properties of β-MnO_2 are investigated using density functional theory with Hubbard U corrections (DFT+U). We find good agreement between the measured experimental voltage, 3.0 V, and our calculated value of 3.2 V. We consider the pathways for lithium migration and find a small barrier of 0.17 eV for bulk β-MnO_2, which is likely to contribute to its good performance as a lithium intercalation cathode in the mesoporous form. However, by explicit calculation of surface to bulk ion migration, we find a higher barrier of >0.6 eV for lithium insertion at the (101) surface that dominates the equilibrium morphology. This is likely to limit the practical use of bulk samples, and demonstrates the quantitative importance of surface to bulk ion migration in Li ion cathodes and supercapacitors. On the basis of the calculation of the electrostatic potential near the surface, we propose an efficient method to screen systems for the importance of surface migration effects. Such insight is valuable for the future optimization of manganese oxide nanomaterials for energy storage devices.

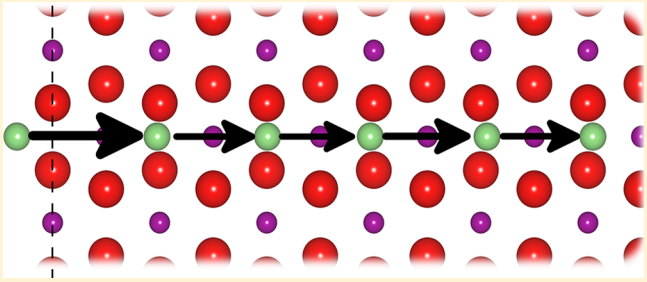

KEYWORDS: *lithium battery, surface, supercapacitor, DFT, cathode, manganese oxides*

INTRODUCTION

Energy storage for hybrid electric vehicles and renewable energy sources is a pressing technological challenge for which Li ion batteries and supercapacitors are key candidate systems. Due to rising future needs, there has been an intensive research effort to search for an alternative to the layered $LiCoO_2$ system conventionally used in rechargeable Li ion batteries.[1−4] Co-based materials pose problems due to high cost and environmental hazards upon disposal. Therefore, manganese-based oxides have been a promising class of materials for electrochemical energy storage.[5−10]

β-MnO_2 has been extensively investigated as a cathode for rechargeable Li ion cells, but early work showed that bulk samples did not permit significant Li ion intercalation.[7,10,11] Initial work on β-MnO_2 supercapacitors[12] also indicated lower capacitance than for other polymorphs such as hollandite MnO_2. Yet recent investigations have reinvigorated interest in the material. Mesoporous[10,13,14] and needle-like nanostructured[15,16] β-MnO_2 have been shown to allow good intercalation of Li ions. Both pore size and wall thickness of the mesoporous structures have been demonstrated to affect the rate capability.[9] The mesoporous β-MnO_2 cell has a capacity[10] of 284 mAh/g and good cycling stability. Recent studies of kinetics using ac impedance measurements[17] have demonstrated increased Li ion diffusion in nanosized materials. Additionally, β-MnO_2 has shown promise as a catalyst for the oxygen reduction reaction that is the basis of the Li−air battery system[18,19] and as a supercapacitor electrode material.[12,20] The formation of nanostructured small particles has been shown to dramatically increase the capacitance[20] of β-MnO_2 to 294 F g^{-1}, compared to ∼9 F g^{-1} for bulk cyrstals.[12]

However, the fundamental basis for the constrasting intercalation properties of nanostructured mesoporous β-MnO_2 and bulk crystalline β-MnO_2 is not fully understood. To understand the factors influencing their electrochemical and nanoionic behavior, it is clear that greater knowledge of the diffusion pathways and activation energies that govern Li ion mobility within the bulk and at the surface is needed on the atomic scale. Motivated by renewed interest in β-MnO_2, we performed an *ab initio* study of its intercalation behavior extending our recent computational work on lithium battery materials.[21,22] Of key interest is how mesoporous structuring enables intercalation into β-MnO_2. Indeed, the rapidly growing interest in nanostructuring of many electrode materials[23,24] calls for investigation of the influence of surfaces and interfaces. It is known that, in many cases, nanomaterials have enabled higher intercalation/deintercalation rates (and hence higher power) by reducing the diffusion path length to facilitate fast Li ion

Received: October 12, 2012
Revised: January 21, 2013
Published: January 22, 2013

transport and by increasing the surface area to promote Li ion exchange across the electrode/electrolyte boundary.

We organize our results as follows. First, results on the prediction of the Li ion intercalation voltage and the associated structural changes are compared to experiment. We then consider transition state calculations of the Li ion migration properties in bulk migration of β-MnO_2. Finally, we explicitly treat the migration from the surface to bulk in β-MnO_2.

Figure 1 shows the crystal structure of β-MnO_2 where the approximate MnO_6 octahedra are indicated by polyhedra. β-MnO_2 occurs in the rutile structure[25] with only corner-sharing octahedra in-plane that create 1 × 1 tunnels clearly visible along the c-axis in Figure 1a. These tunnels are expected to play a key role in the ion migration considered in this work. Migration paths A and B in Figure 1a involve movement between these tunnels, while path C in Figure 1b is characterized by movement along these tunnels. We will return to consider the energetics of these migration paths in detail.

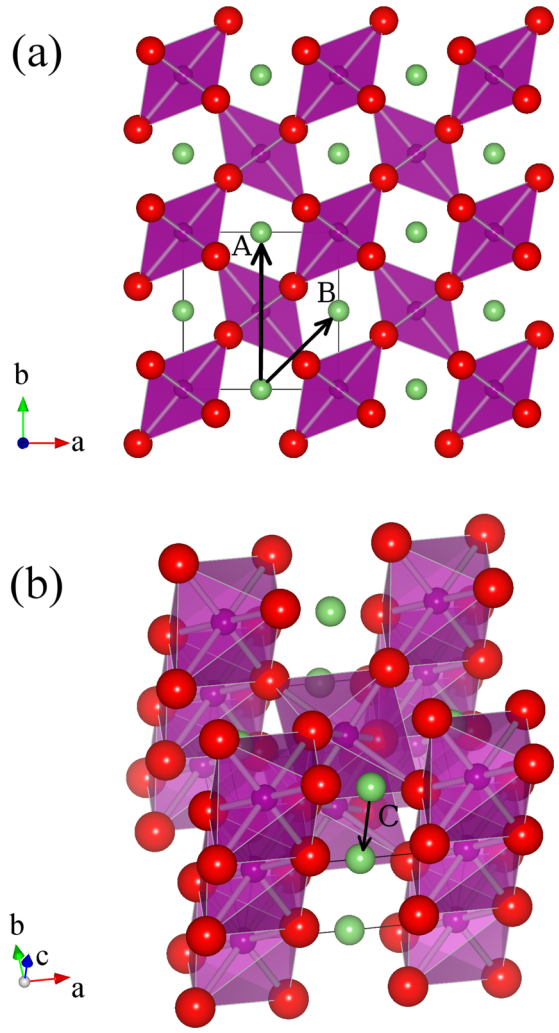

Figure 1. Crystal structure of β-MnO_2 showing the connecting MnO_6 octahedra and the intercalated Li ions viewed (a) along the c-axis and (b) obliquely. Red spheres are oxygen, purple manganese, and green lithium. The thin black lines indicate the conventional unit cell. Migration paths indicated by bold arrows are associated with the calculated migration barriers in Table 2.

Lithium insertion into mixed β-MnO_2 and ramsdellite MnO_2 has previously been studied by Maphanga et al. using interatomic force field methods.[26] In that work, finite temperature molecular dynamics calculations indicated the presence of increased twinning and a tendency to form ramsdellite units upon the intercalation of lithium. Sayle et al.[27] have also investigated β-MnO_2 using interatomic potentials and have considered the microstructure, nanoparticle formation, and mechanical properties in detail using large-scale molecular dynamics methods.

Previous DFT-based studies on β-MnO_2 have considered hydrogen insertion,[28] the phase stability of competing polymorphs,[29] Ruetschi defects in nanosheets,[30] and magnetic properties.[31,32] Given the promising experimental results for intercalation of Li ions into mesoporous β-MnO_2, there is a need to extend these studies to understand the Li ion intercalation processes, in particular, to determine why nanostructured and mesoporous crystals may improve the properties so greatly.

Koudriachova et al. have previously studied the intercalation properties of nanostructured rutile TiO_2 by *ab initio* methods. This work highlighted anisotropic diffusion and the ability of local structural distortions to create Li ion traps that inhibit diffusion.[33] They also argued that short diffusion lengths and increased structural flexibility near the surface of nanostructures reduce these effects.[34]

METHODS

We have calculated the electronic structure using the generalized gradient approximation[35] (GGA) with Hubbard U corrections GGA +U. The VASP[36] code was employed using PAW potentials. The cutoff for the planewave basis set was 520 eV. A minimum of 6 × 6 × 6 k-points was used for each calculation. Where stated in the results, the all-electron full-potenial code Wien2k[37] was also employed. Here RK_{max} was set to 7.0 and the radii of the muffin tins was 2.01 a_0 for manganese, 1.51 a_0 for oxygen, and 1.51 a_0 for lithium.

The value of the U parameter for our GGA+U calculations was determined *ab initio* using Wien2k.[38,39] For β-MnO_2, we obtain U_{Eff} = 5.5 eV and after lithium intercalation we obtain U_{Eff} = 4.7 eV for Li-β-MnO_2. To obtain intercalation voltages we require a single value of U for both the delithiated and lithiated materials. We therefore follow the practice in previous studies[40] and use the average from the two calculations, $U_{Eff} = (U - J) = 5.1$ eV, for the spherical part of the interaction for the remainder of this study. All calculations were performed in a ferromagnetic spin polarized configuration with the fully localized limit double counting correction.[41] Since the exchange interaction is poorly screened in solids,[38,42] we employ an atomic limit value J = 1.0 eV for β-MnO_2, an approach extensively justified in previous work.[43]

RESULTS AND DISCUSSION

Structures and Voltages. Pristine β-MnO_2 occurs in the tetragonal space group $P4/mnm$ (No. 136) with lattice parameters[44] $a = b = 4.398$ Å and $c = 2.873$ Å. Intercalation of Li ions in mesoporous β-MnO_2 occurs by a two-phase reaction on first discharge[9] to form β-$LiMnO_2$ with a voltage of approximately 3.0 V.[10] X-ray diffraction results[45] indicate that the intercalation reduces the tetragonal symmetry to orthorhombic space group $Pnnm$ (No. 58). The lattice parameters are a = 5.1419(7) Å, b = 5.003(2) Å, and c = 2.8131(8) Å, representing a contraction of the c-axis with an accompanying expansion in-plane. This is attributed to the Jahn−Teller distortion when Li ion intercalation causes Mn^{4+} to become Mn^{3+}.

In Table 1 we show the GGA+U predicted lattice parameters for β-MnO_2 and its lithiated structure via a two-phase reaction. If we first consider β-MnO_2, the lattice parameters predicted by

dx.doi.org/10.1021/cm303295f | Chem. Mater. 2013, 25, 536−541

Table 1. Calculated and Experimental[10,45] Lattice Parameters for β-MnO_2 and Its Lithiated Form and Cell Voltages for β-$LiMnO_2$

	a (Å)	b (Å)	c (Å)	V (V)
		β-MnO_2		
GGA+U	4.442	4.442	2.933	–
expt	4.398	4.398	2.873	–
		β-$LiMnO_2$		
GGA+U	5.204	5.148	2.853	3.2
expt	5.141	5.003	2.813	3.0

GGA+U agree with those from experiment to within 3%, but the usual tendency for GGA+U to overestimate the unit cell volume is evident. For the lithiated β-$LiMnO_2$ structure, the Jahn–Teller distortion experimentally results in a c-axis reduced by 2% while the a-axis has expanded by 17% and the b-axis by 14%. The GGA+U results shown in Table 1 also predict this contracted structure. All of the GGA+U lattice parameters lie within 3% of those from experiment. It should be noted that the experimental data for β-$LiMnO_2$ is derived from mesoporous samples and this may affect the structure.

Experimentally, the intercalation voltage of mesoporous β-MnO_2 is 3.0 V[10] for the two-phase process. From our GGA+U total energy calculations for bulk β-MnO_2 we obtain a value of 3.2 V. The small difference between our GGA+U result and experiment is typical of the accuracy obtained with this method over a large class of intercalation compounds.[46] Furthermore, structural contributions to the total energy due to the mesoporous structure are not accounted for in our calculations. Nevertheless, despite the fact that bulk β-MnO_2 permits little intercalation experimentally, the accuracy of our calculated voltage indicates good reproduction of the key contributions to the thermodynamics of intercalation in mesoporous β-MnO_2. The result also makes clear that the inability to intercalate into bulk β-MnO_2 is not because the process is thermodynamically unfavorable but is due to kinetic barriers.

Bulk Migration. Lithium migration properties are important to the rate at which a battery may charge/discharge and hence deliver power. Materials may intercalate with suitable thermodynamics for the voltage, but poor migration rate properties can render them of no practical use, such as MoO_3.[47,48] Understanding the difficulty of inserting even minor amounts of lithium into bulk β-MnO_2 is a key problem.

In Figure 1 we show the three probable paths for migration of Li ions in the dilute limit of bulk β-MnO_2. Path A corresponds to migration in the a,b-plane (along [010] and symmetry equivalent [100]). Path B is migration simultaneously along the c-axis and in the a,b-plane (along [111] and symmetry equivalent paths). Path C is migration along the 1 × 1 c-axis tunnel (directed along [001]). Using the nudged elastic band method the migration barriers were calculated in the dilute limit of a 4 × 4 × 6 supercell corresponding to one lithium in a unit cell of 192 formula units.

Table 2 lists the migration barriers. It is clear that migration along the c-axis (path C) is the most favorable path, with a barrier of 0.17 eV. Paths A and B both involve migration between 1 × 1 tunnels and possess very high migration barriers >2 eV. This is due to the fact that migration between the c-axis tunnels requires large distortion of the MnO_6 octahedra, which incurs a large energy cost. Our migration barriers therefore imply that lithium diffusion in bulk β-MnO_2 is primarily one-dimensional (1D). Large anisotropy in Li ion diffusion has also been observed experimentally[49] and from *ab initio* calculations[50] in rutile TiO_2. Furthermore, previous work on olivine materials[51,52] has emphasized the capacity for 1D diffusion to make Li ion transport susceptible to blocking defects. The tendency for polymorphism, microtwinning, and grain boundary formation in MnO_2 has also been highlighted[27] for its influence on the intercalation properties of bulk β-MnO_2.

Table 2. Energy Barriers and Li–Li Distances for the Lithium Migration Paths in Bulk β-MnO_2 Shown in Figure 1

path	description	ΔE (eV)	dist (Å)
A	along [010]	7.33	4.44
B	along [111]	2.22	3.48
C	along [001]	0.17	2.94

The low migration barrier of 0.17 eV for path C indicates why the rate performance of the mesoporous form of β-MnO_2 is so good. Jiao et al.[10] found that the dishcarge capacity fell by only 19% when the discharge rate is increased from 15 to 300 mA/g. Also, since the facile c-axis migration in bulk β-MnO_2 is principally along the c-axis, it is likely that lithium may only enter the material via surfaces with a component perpendicular to this direction. The mesoporous and nanosized crystals that allow cycling are likely to give greater exposure of these surfaces, a topic we will return to.

Surface to Bulk Migration. The importance of surfaces and interfaces to both ionic and electronic conductivity in nanoionic materials has been highlighted.[53] The influence of Li ion migration at surfaces on electrode kinetics may be explored using theoretical means. However, while surface energies and morphologies of cathode materials have previously been studied,[54−56] explicit work on Li ion migration barriers at surfaces is lacking.

In Figure 2 we show an adaptation of the equilibrium crystal morphology determined by using interatomic potential methods.[57] The simulated morphology is consistent with the macroscopic shape of β-MnO_2 determined by scanning electron microscopy (SEM).[18,58,59] Figure 2a shows an oblique view, while Figure 2b shows a view along c-axis and demonstrates that access to the route of facile c-axis migration is only available at the (101) and symmetry equivalent surfaces. The prominence of the (101) surface is consistent with previous ab intitio work on rutile MnO_2[60] and TiO_2.[61] Consequently, it is likely that this is the surface through which most lithium must migrate into bulk crystals.

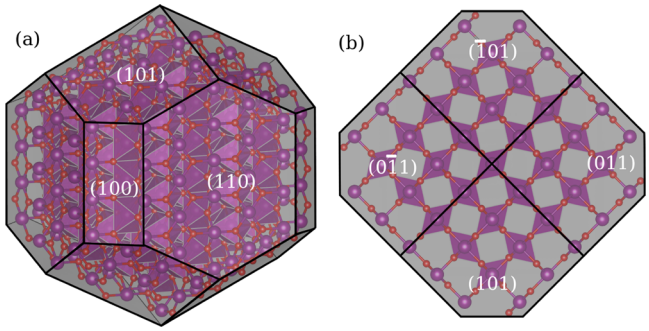

Figure 2. The predicted equilibrium morphology[57] of β-MnO_2 (a) from an oblique view and (b) along the c-axis. Adapted from the results of ref 57.

dx.doi.org/10.1021/cm303295f | *Chem. Mater.* 2013, 25, 536–541

Using a slab of 288 atoms [cleaved with symmetric (101) surfaces terminated by an oxygen layer and having a vacuum of 12 Å], the Li ion migration from the surface to the bulk-like slab center has been studied using VASP. One lithium atom was inserted into this slab and the total energy with full structural relaxation evaluated at 42 depths of insertion between the surface and center of the slab. Constrained minimization was used to hold the depth of the Li ion fixed while all other degrees of freedom were relaxed. The results are shown in Figure 3. The key finding is that the initial barrier to Li ion

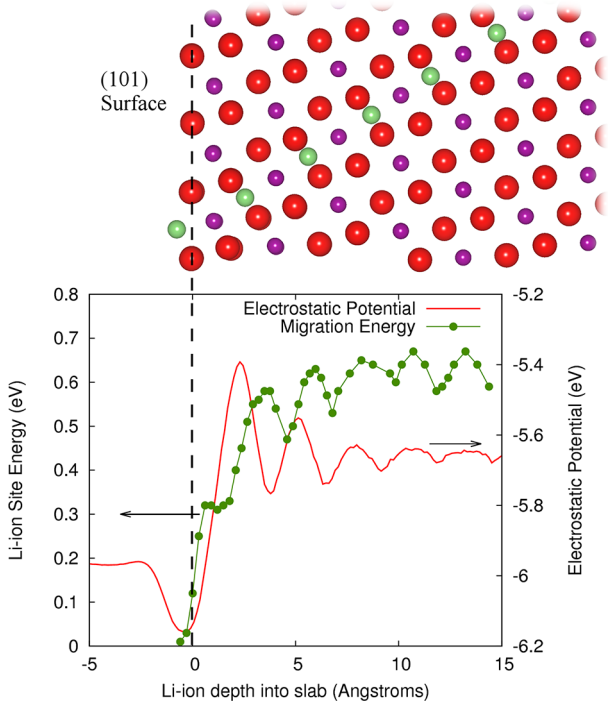

Figure 3. The surface to bulk Li ion migration barrier at the (101) surface of β-MnO_2 is shown along with the corresponding electrostatic potential in the lower panel. Upper panel schematically shows the migration path from this surface. Red spheres are oxygen, purple manganese, and green lithium. The green line is a guide to the eye. The vertical dashed line at zero depth is aligned with the outermost oxygen layer.

insertion at the surface is >0.6 eV, which is much greater than the bulk migration energy of 0.17 eV. The small plateau in the Li ion site energy at a depth of ~1.3 Å has an energy well that is too shallow to be a stable lattice site. This barrier of >0.6 eV occurs predominantly over the first 5 Å after the Li ion passes the outermost surface oxygen layer. Furthermore, between 10 and 15 Å in depth it can be seen that the migration is becoming bulk-like with a barrier close to 0.17 eV.

In addition to the migration barrier calculated from total energies, Figure 3 also depicts the electrostatic potential experienced by a positive charge with the formal charge +1*e* of a Li ion along the path of the migration. This has been calculated by the sum of the ionic and Hartree potentials in a delithiated slab. The ionic potential is due to the nuclear charge and core electrons. The Hartree potential is the electrostatic potential due to the valence electrons in the system, the distribution of which is calculated explicity by the density functional theory method we employ. From Figure 3 it is clear that there is a strong correspondence between the locations of the peaks in the electrostatic potential and the peaks in the plot of the Li ion site energy. However, the associated electron is able to screen the potential from the Li ion. Furthermore, effects of chemical bonding will influence the site energy, and these factors together make the correspondence, while useful and computationally efficient, qualitative. From the correspondence outlined above, the Li ion site energies near the surface in Figure 3 appear to be predominantly affected by the large oscillations in the electrostatic potential. As the ion passes further toward the bulk, the oscillations in electrostatic potential become smaller and will still influence the site energy. However, bonding and structural relaxation effects may then have a proportionately greater role in determining the site energy as we approach the bulk-like region.

As well as the surface potential, structural strain as the lithium ion enters the surface may be a contributing factor. To quantify the strain we have calculated the ionic displacements of the near neighbors to the lithium ions at depths of 0, 2, 4.5, and 9.5 Å. The results are shown in Table 3. The displacements

Table 3. Displacements of Near Neighbors to the Li Ion at Intercalation Depths of −0.7, 2, 4.5, and 9.5 in Å from the (101) Surface[a]

	displacements			
	−0.7 Å	2 Å	4.5 Å	9.5 Å
O1-coplanar	NA	0.143	0.145	0.159
O2-coplanar	0.000	0.144	0.140	0.158
O3	0.000	0.121	0.106	0.109
O4	NA	0.166	0.105	0.116
O5	0.000	0.052	0.105	0.078
O6	NA	0.175	0.096	0.121
Mn1-coplanar	NA	0.261	0.168	0.141
Mn2-coplanar	NA	0.138	0.144	0.142
average	0.000	0.150	0.126	0.128

[a]Depths measured relative to the outermost oxygen layer, consistent with the scale in Figure 3. The coplanar oxygen atoms are in the same plane as the Li ion, the plane being drawn perpendicular to the direction of migration. Note that the surface adsorbed lithium at −0.7 Å is three-fold coordinate; therefore, some near neighbors are not applicable (NA).

for all depths beyond the surface are nonzero, but it is clear that the displacements in the bulk-like region near 9.5 Å, averaging 0.128 Å, are similar to those near the surface at 2 and 4.5 Å with averages of 0.150 and 0.126 Å, respectively. Therefore, we argue that the main barrier between the surface and bulk is due to the surface electrostatic potential rather than structural strain.

To assess the surface to bulk migration barrier at alternative surfaces the (001) surface has been considered. The (001) surface was chosen as it is calculated[57] to have the lowest energy, after (101), among surfaces giving access to the tunnel for *c*-axis migration. The other surfaces of lower energy, (110) and (100), do not give access to the *c*-axis tunnel due to the high migration barriers A and B presented in Table 2.

It is useful to discuss some general properties of the two surfaces we treat, namely the (101) and the (001). According to the classification of Tasker,[62] "as-cut" surfaces can be one of three structural types, which are normally referred to as types I, II, and III. Type I surfaces are formed from layers containing a charge-neutral combination of cations and anions and thus have no net dipole perpendicular to the surface plane. For type II surfaces, a finite group of atomic layers parallel to the surface form a charge-neutral, repeated unit with no net dipole normal

dx.doi.org/10.1021/cm303295f | *Chem. Mater.* 2013, 25, 536−541

to the surface normal. For type III surfaces, by contrast, irrespective of where the crystal is cut, a dipole moment always exists perpendicular to the surface plane; in this case, convergent surface energies can only be obtained if the surface layer is reconstructed in some way to remove the dipole moment. This usually involves removing a suitable number of ions from one side of the crystal to the other in order to make the crystal slab symmetric about its midpoint. In this scheme, the (101) surface of β-MnO_2 falls into the type II category, with a repeat unit of three layers oxygen−manganese−oxygen lying parallel to the surface. The (001) surface, however, is type I with charge neutral MnO_2 layers parallel to the surface.

Figure 4 shows the migration barrier profile calculated using constrained minimization for the (001) surface. The largest

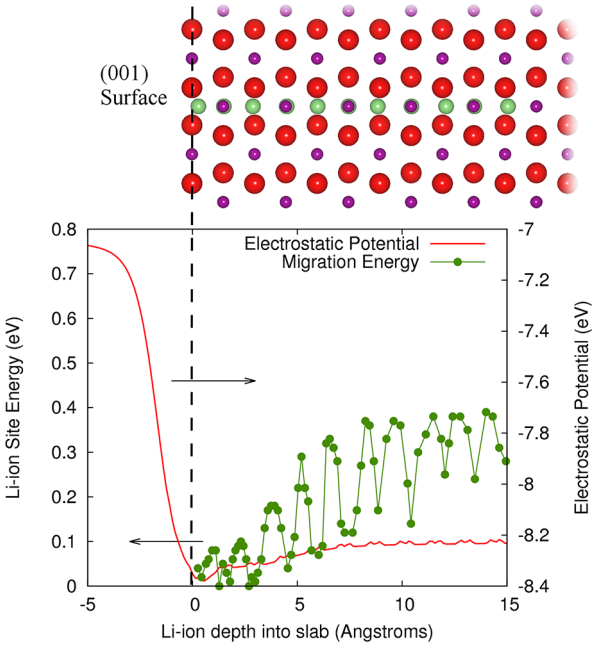

Figure 4. The surface to bulk Li ion migration barrier at the (001) surface of β-MnO_2 is shown along with the corresponding electrostatic potential in the lower panel. The upper panel schematically shows the migration path from this surface. Red spheres are oxygen, purple manganese, and green lithium. The green line is a guide to the eye. The vertical dashed line at zero depth is aligned with the outermost oxygen layer.

single barrier, near a depth of 6 Å, is less than 0.3 eV. It is clear that the barrier to migration at this surface is much smaller than at the (101) surface. The electrostatic potential associated with the type I (001) surface possesses only small variations compared to that due to the type II (101) surface. Consequently, the metal−oxygen layers dominate and we see a peak in the migration barrier profile as the lithium passes each one. Upon the basis of this correspondence, we suggest that the form of the electrostatic potential in the near surface regions may be used to efficiently screen systems for the importance of surface migration effects. It is argued that nanostructuring is capable of exposing alternative surfaces, such as the (001), and that this is a means via which intercalation processes may be enhanced in both Li ion batteries and supercapacitors.

A further consideration is that in real battery and supercapacitor systems these surfaces will be surrounded by electrolyte solutions. The charged ions in solution may become adsorbed to surface sites, particularly at the partial charges of the oxygen-terminated surfaces.[63] This adsorption is likely to alter the form of the surface potential and will be the subject of future investigation. The precise nature of the effects will depend upon the pH and other characteristics of the electrolyte solution. However, we suggest that due to the finite size of adsorbed ions the addition of a Stern-type charge layer will largely affect the electrostatic potential in the region outside the surface, while the primary contribution to the migration barriers in Figures 3 and 4 occurs in the initial subsurface layers.

It is stressed that we have investigated key low-energy surfaces that allow access to the favored *c*-axis tunnel for Li ion diffusion. Clearly other surfaces may be exposed by nanostructuring, but due to the very large computational demands of these calculations, their treatment warrants future studies. Nevertheless, this work demonstrates quantitatively that the migration barrier at surfaces can be the limiting process for ion intercalation. Furthermore, given that supercapacitors rely upon ion intercalation for much of their capacitance, it is likely that the same influences are active in β-MnO_2 supercapacitors. It is likely that the impact of surfaces upon the Li ion migration characteristics is significant in other cathode and anode materials, and this will be the subject of future work.

CONCLUSIONS

This investigation has provided new atomic-scale insights into the intercalation properties of β-MnO_2, especially the importance of considering surface effects. The key results include the following:

(1) GGA+U shows good reproduction of experimental crystal structures, including Jahn−Teller distortions, and lithium intercalation voltages.

(2) The migration of Li ions in bulk β-MnO_2 is primarily one-dimensional along the *c*-axis tunnels in the rutile structure, indicating anisotropic diffusion.

(3) The Li ion migration barrier from the (101) surface to bulk is >0.6 eV and dominates over the bulk migration barrier of 0.17 eV. This surface migration barrier is likely to influence the difficulty in intercalating lithium into bulk samples of β-MnO_2 and suggests why intercalation is switched on by moving to nanostructured crystals. Indeed, such intrinsic differences in the Li ion mobility in the bulk and at the surfaces may be key factors in the intercalation behavior of nanostructured versus bulk crystalline systems for many materials.

(4) On the basis of the calculation of the electrostatic potential near the surface and its correlation with the Li ion migration at that surface, we suggest an efficient means to screen systems for the importance of surface migration effects.

(5) This work is a quantitative demonstration of a rate-limiting surface to bulk ion migration barrier, which is significant for the kinetics of intercalation/deintercalation and hence for charge/discharge rates.

(6) These results suggest that synthesis techniques such as nanosizing that are capable of exposing alternative surfaces may enhance intercalation processes in both battery and supercapacitor systems.

Given the importance of understanding the ion intercalation process, the results presented in this paper provide valuable insight for the future optimization of nanostructured manganese oxides for energy storage devices.

dx.doi.org/10.1021/cm303295f | *Chem. Mater.* 2013, 25, 536−541

AUTHOR INFORMATION

Corresponding Author

*E-mail: dt331@bath.ac.uk (D.A.T.); m.s.islam@bath.ac.uk (M.S.I.).

Notes

The authors declare no competing financial interest.

ACKNOWLEDGMENTS

We are grateful to the EPSRC for funding (EP/H019596; EP/H003819) and to the Materials Chemistry Consortium for Hector supercomputer resources.

REFERENCES

(1) Tarascon, J. M.; Delacourt, C.; Prakash, A. S.; Morcrette, M.; Hegde, M. S.; Wurm, C.; Masquelier, C. *Dalton Trans.* **2004**, 2988−2994.
(2) Ellis, B. L.; Lee, K. T.; Nazar, L. F. *Chem. Mater.* **2010**, *22*, 691.
(3) Goodenough, J. B.; Kim, Y. *Chem. Mater.* **2010**, *22*, 587−603.
(4) Whittingham, M. S.; Savinell, R. F.; Zawodzinski, T. *Chem. Rev.* **2004**, *104*, 4243−4244.
(5) Armstrong, A. R.; Bruce, P. G. *Nature* **1996**, *381*, 499−500.
(6) Tarascon, J.; Wange, E.; Shokoohi, F.; McKinnon, W.; Colson, S. *J. Electrochem. Soc.* **1991**, *138*, 2859−2864.
(7) Thackeray, M. M. *Prog. Solid State Chem.* **1997**, *25*, 1−71.
(8) Armstrong, A. R.; Holzapfel, M.; Novak, P.; Johnson, C. S.; Kang, S. H.; Thackeray, M. M.; Bruce, P. G. *J. Am. Chem. Soc.* **2006**, *128*, 8694−8698.
(9) Ren, Y.; Armstrong, A. R.; Jiao, F.; Bruce, P. G. *J. Am. Chem. Soc.* **2010**, *132*, 996−1004.
(10) Jiao, F.; Bruce, P. G. *Adv. Mater.* **2007**, *19*, 657.
(11) Kijima, N.; Sakata, Y.; Takahashi, Y.; Akimoto, J.; Kumagai, T.; Igarashi, K.; Shimizu, T. *Solid State Ionics* **2009**, *180*, 616−620.
(12) Devaraj, S.; Munichandraiah, N. *J. Phys. Chem. C* **2008**, *112*, 4406.
(13) Luo, J.-Y.; Zhang, J.-J.; Xia, Y.-Y. *Chem. Mater.* **2006**, *18*, 5618−5623.
(14) Mathew, V.; Lim, J.; Kang, J.; Gim, J.; Rai, A. K.; Kim, J. *Electrochem. Commun.* **2011**, *13*, 730−733.
(15) Cheng, F. Y.; Zhao, J. Z.; Song, W.; Li, C. S.; Ma, H.; Chen, J.; Shen, P. W. *Inorg. Chem.* **2006**, *45*, 2038−2044.
(16) Tang, W. P.; Yang, X. J.; Liu, Z. H.; Ooi, K. *J. Mater. Chem.* **2003**, *13*, 2989−2995.
(17) Bach, S.; Pereira-Ramos, J. P.; Willmann, P. *Electrochim. Acta* **2011**, *56*, 10016.
(18) Debart, A.; Paterson, A. J.; Bao, J.; Bruce, P. G. *Angew. Chem., Int. Ed.* **2008**, *47*, 4521−4524.
(19) Thapa, A. K.; Hidaka, Y.; Hagiwara, H.; Ida, S.; Ishihara, T. *J. Electrochem. Soc.* **2011**, *158*, A1483−A1489.
(20) Zang, J.; Li, X. *J. Mater. Chem.* **2011**, *21*, 10965−10969.
(21) Armstrong, A. R.; Kuganathan, N.; Islam, M. S.; Bruce, P. G. *J. Am. Chem. Soc.* **2011**, *133*, 13031.
(22) Eames, C.; Armstrong, A. R.; Bruce, P. G.; Islam, M. S. *Chem. Mater.* **2012**, *24*, 2155.
(23) Ren, Y.; Hardwick, L. J.; Bruce, P. G. *Angew. Chem., Int. Ed.* **2010**, *49*, 2570−2574.
(24) Lee, K. T.; Cho, J. *Nano Today* **2011**, *6*, 28−41.
(25) Baur, W. H. *Acta Crystallagr. B* **1976**, *32*, 2200.
(26) Maphanga, R. R.; Sayle, D. C.; Sayle, T. X. T.; Ngoepe, P. E. *Phys. Chem. Chem. Phys.* **2011**, *13*, 1307.
(27) (a) Sayle, T. X. T.; Maphanga, R. R.; Ngoepe, P. E.; Sayle, D. C. *J. Am. Chem. Soc.* **2009**, *131*, 6161−6173. (b) Sayle, T. X. T.; Catlow, C. R. A.; Maphanga, R. R.; Ngoepe, P. E.; Sayle, D. C. *J. Cryst. Growth* **2006**, *294*, 118−129. (c) Sayle, T. X. T.; Catlow, C. R. A.; Maphanga, R. R.; Ngoepe, P. E.; Sayle, D. C. *J. Am. Chem. Soc.* **2005**, *127*, 12828−12837. (d) Sayle, T. X. T.; Ngoepe, P. E.; Sayle, D. C. *ACS Nano* **2009**, *3*, 3308−3314.
(28) Balachandran, D.; Morgan, D.; Ceder, G. *J. Solid State Chem.* **2002**, *166*, 91−103.
(29) Balachandran, D.; Morgan, D.; Ceder, G.; van de Walle, A. *J. Solid State Chem.* **2003**, *173*, 462−475.
(30) Kwon, K. D.; Refson, K.; Sposito, G. *Phys. Rev. Lett.* **2008**, *100*, 146601.
(31) Franchini, C.; Podloucky, R.; Paier, J.; Marsman, M.; Kresse, G. *Phys. Rev. B* **2007**, *75*, 195128.
(32) Mackrodt, W. C.; Williamson, E.-A. *J. Chem. Soc., Faraday Trans.* **1997**, *93*, 3295−3300.
(33) Koudriachova, M. V.; Harrison, N. M.; de Leeuw, S. W. *Phys. Rev. Lett.* **2001**, *86*, 1275.
(34) Koudriachova, M. V. *J. Power Sources* **2011**, *196*, 6898.
(35) Perdew, J.; Burke, K.; Ernzerhof, M. *Phys. Rev. Lett.* **1996**, *77*, 3865.
(36) Kresse, G.; Furthmüller, J. *Phys. Rev. B* **1996**, *54*, 11169−11186.
(37) Schwarz, K.; Blaha, P. *Comput. Mater. Sci.* **2003**, *28*, 259.
(38) Anisimov, V. I.; Zaanen, J.; Andersen, O. K. *Phys. Rev. B* **1991**, *44*, 943−954.
(39) Madsen, G. K. H.; Novak, P. *Europhys. Lett.* **2005**, *69*, 777.
(40) Zhou, F.; Cococcioni, M.; Marianetti, C. A.; Morgan, D.; Ceder, G. *Phys. Rev. B* **2004**, *70*, 235121.
(41) Ylvisaker, E. R.; Pickett, W. E.; Koepernik, K. *Phys. Rev. B* **2009**, *79*, 035103.
(42) Antonides, E.; Janse, E. C.; Sawatzky, G. A. *Phys. Rev. B* **1977**, *15*, 1669−1679.
(43) Tompsett, D. A.; Middlemiss, D. S.; Islam, M. S. *Phys. Rev. B* **2012**, *86*, 205126.
(44) Regulski, M.; Przeniosło, R.; Sosnowska, I.; Hoffmann, J.-U. *J. Phys. Soc. Jpn.* **2004**, *73*, 3444−3447.
(45) Ren, Y. Ph.D. Thesis, University of St. Andrews, 2010.
(46) Chevrier, V. L.; Ong, S. P.; Armiento, R.; Chan, M. K. Y.; Ceder, G. *Phys. Rev. B* **2010**, *82*, 075122.
(47) Whittingham, M. S.; Dines, M. B. *J. Electrochem. Soc.* **1977**, *124*, 1387−1388.
(48) Whittingham, M. S. *J. Electrochem. Soc.* **1976**, *123*, 315−320.
(49) Johnson, O. W. *Phys. Rev.* **1964**, *136*, A284.
(50) Koudriachova, M. V.; Harrison, N. M.; de Leeuw, S. W. *Solid State Ionics* **2003**, *157*, 35.
(51) Islam, M. S.; Driscoll, D. J.; Fisher, C. A. J.; Slater, P. R. *Chem. Mater.* **2005**, *17*, 5085−5092.
(52) Morgan, D.; der Ven, A. V.; Ceder, G. *Electrochem. Solid-State Lett.* **2004**, *7*, A30−A32.
(53) Maier, J. *Nat. Mater.* **2005**, *4*, 805−815.
(54) Wang, L.; Zhou, F.; Meng, Y. S.; Ceder, G. *Phys. Rev. B* **2007**, *76*, 165435.
(55) Wang, L.; Zhou, F.; Ceder, G. *Electrochem. Solid State Lett.* **2008**, *11*, A94−A96.
(56) Fisher, C. A. J.; Islam, M. S. *J. Mater. Chem.* **2008**, *18*, 1209.
(57) Maphanga, R. R.; Parker, S. C.; Ngoepe, P. E. *Surf. Sci.* **2009**, *603*, 3184−3190.
(58) Guan, H.; Chen, G.; Zhu, J.; Wang, Y. *J. Alloys Compd.* **2010**, *507*, 126−132.
(59) Zhang, X.; Yang, W.; Yang, J.; Evans, D. G. *J. Cryst. Growth* **2008**, *310*, 716.
(60) Oxford, G. A. E.; Chaka, A. M. *J. Phys. Chem. C* **2011**, *115*, 16992−17008.
(61) Ramamoorthy, M.; Vanderbilt, D.; Kingsmith, R. D. *Phys. Rev. B* **1994**, *49*, 16721−16727.
(62) Tasker, P. W. *J. Phys. C: Solid State Phys.* **1979**, *12*, 4977.
(63) Butt, H.-J.; Graf, K.; Kappl, M. *Physics and Chemistry of Interfaces*; Wiley-VCH: Weinheim, Germany, 2006.